Biomechanical evaluation of different semi-rigid junctional fixation techniques using finite element analysis

Document Version:
Publisher's PDF, also known as Version of Record (includes final page, issue and volume numbers)

Please check the document version of this publication:

• A submitted manuscript is the version of the article upon submission and before peer-review. There can be important differences between the submitted version and the official published version of record. People interested in the research are advised to contact the author for the final version of the publication, or visit the DOI to the publisher's website.
• The final author version and the galley proof are versions of the publication after peer review.
• The final published version features the final layout of the paper including the volume, issue and page numbers.

Link to publication

Download date: 17. Nov. 2023

Biomechanical evaluation of different semi-rigid junctional fixation techniques using finite element analysis

Julia L. van Agtmaal [a,b], Remco J.P. Doodkorte [b], Alex K. Roth [b], Keita Ito [a], Jacobus J.C. Arts [a,b], Paul C. Willems [b], Bert van Rietbergen [a,b,*]

[a] *Orthopaedic Biomechanics, Department of Biomedical Engineering, Eindhoven University of Technology, Den Dolech 2, 5612AZ Eindhoven, the Netherlands*
[b] *Department of Orthopaedic Surgery, Research School CAPHRI, Maastricht University Medical Center, P. Debyelaan 25, 6229HX Maastricht, the Netherlands*

ABSTRACT

Background: Proximal junctional failure is a common complication attributed to the rigidity of long pedicle screw fixation constructs used for surgical correction of adult spinal deformity. Semi-rigid junctional fixation achieves a gradual transition in range of motion at the ends of spinal instrumentation, which could lead to reduced junctional stresses, and ultimately reduce the incidence of proximal junctional failure. This study investigates the biomechanical effect of different semi-rigid junctional fixation techniques in a T8-L3 finite element spine segment model.
Methods: First, degeneration of the intervertebral disc was successfully implemented by altering the height. Second, transverse process hooks, one- and two-level clamped tapes, and one- and two-level knotted tapes instrumented proximally to three-level pedicle screw fixation were validated against *ex vivo* range of motion data of a previous study. Finally, the posterior ligament complex forces and nucleus pulposus stresses were quantified.
Findings: Simulated range of motions demonstrated the fidelity of the general model and modelling of semi-rigid junctional fixation techniques. All semi-rigid junctional fixation techniques reduced the posterior ligament complex forces at the junctional zone compared to pedicle screw fixation. Transverse process hooks and knotted tapes reduced nucleus pulposus stresses, whereas clamped tapes increased nucleus pulposus stresses at the junctional zone.
Interpretation: The relationship between the range of motion transition and the reductions in posterior ligament complex and nucleus pulposus stresses was complex and dependent on the fixation techniques. Clinical trials are required to compare the effectiveness of semi-rigid junctional fixation techniques in terms of reducing proximal junctional failure incidence rates.

1. Introduction

Spinal fusion with segmental pedicle screw fixation (PSF) is the mainstay surgical correction of adult spinal deformity (ASD). Two of the most prevalent complications after spinal fusion surgery for ASD are proximal junctional kyphosis (PJK) and proximal junctional failure (PJF) (Kim et al., 2012). PJK is defined as a change of $\geq 10°$ in the proximal junctional sagittal Cobb angle compared to the preoperative value (Glattes et al., 2005). PJK occurs in approximately 20%–40% of the surgically treated patients, mostly within the first two years after fusion (DeWald and Stanley, 2006; Kim et al., 2012). PJF may be defined as an increase in proximal junctional angle of $>15°$, fracture of the uppermost instrumented vertebra (UIV) or UIV $+$ 1, failure of UIV

instrumentation, or the need for proximal extension of fusion within 6 months postoperatively (Spina et al., 2017).

The pathophysiology behind PJK and PJF is debatable. Resection of the posterior ligament complex (PLC) during surgery may be of influence, as these ligaments naturally prevent PJK (Cahill et al., 2012). Yagi et al. (Yagi et al., 2011) state that 81% of PJK cases were caused by either disc or ligamentous failure. Furthermore, low bone mineral density (BMD) is a major PJF risk factor as increased vertebral compressive stresses increase the risk for vertebral fractures (Spina et al., 2017). Finally, the abrupt change in range of motion (RoM) is believed to result in increased stresses between the rigid UIV and the supra-adjacent mobile segments, resulting in PJK and/or PJF (Kim et al., 2005). Therefore, it has been postulated that a more gradual change in RoM

leads to a reduction in stresses, and thus a reduced risk for PJK (Cahill et al., 2012).

Several clinical and biomechanical studies have investigated a variety of semi-rigid junctional fixation techniques to reduce construct stiffness at the proximal end of a rigid PSF construct (Doodkorte et al., 2021a). In a recent biomechanical study by Doodkorte et al. (Doodkorte et al., 2021b), multiple semi-rigid junctional fixation techniques were directly compared in an *ex vivo* experimental setup. This study demonstrated the feasibility of achieving a gradual RoM transition zone proximal to a rigid three-level PSF by means of two different sublaminar tapes and one-level transverse process hooks (TPH) (Fig. 1). The sublaminar tapes included one- and two-level clamped sublaminar tape (CT1 and CT2), and one- and two-level knotted sublaminar tape (KT1 and KT2). All semi-rigid junctional fixation techniques provided a more gradual transition zone compared to PSF by reducing the RoM at the junctional levels. However, significant differences in the junctional zone kinematics between the techniques were identified.

The outcome parameters measurable in *ex vivo* experimental studies are generally limited to kinematics. Finite element (FE) modelling offers the potential to measure PLC forces and intervertebral discs (IVDs) stresses. FE modelling could therefore be used to assess the effect of different PJK prophylactic techniques on the RoM and the change in stresses and strains at the UIV + 1.

IVD degeneration plays an essential role in the pathogenesis of ASD and correlates with a decreased RoM (Silva and Lenke, 2010). Therefore, the objectives of this study are: first, to incorporate the degenerative changes of the IVD in an existing FE model of the spine in order to accurately replicate the biomechanical behavior of human cadaveric spine specimens (Meijer, 2011). Second, to simulate TPH, CT1, CT2, KT1 and KT2 as semi-rigid junctional fixation techniques, and validate the *in silico* RoM against the *ex vivo* biomechanical results attained in the study by Doodkorte et al. (Doodkorte et al., 2021b) Finally, to investigate whether the gradual change in RoM arising from different types of instrumentation will reduce PLC and IVD stresses in the proximal junctional zone, which potentially reduces the risk of developing PJK/PJF.

2. Methods

2.1. Biomechanical experiment

Experimental results were obtained from a previous study, that aimed to study instrumentation related complications after long-segment instrumentation for the treatment of adult spinal deformity (Doodkorte et al., 2021b). In summary, seven human cadaveric osteo-ligamentous spine segments (T8-L3, average donor age of 83.1 years) were tested in seven different conditions: the native condition, three-level PSF, and three-level PSF supplemented with five different semi-rigid junctional fixation techniques, namely TPH, KT1, KT2, CT1, and CT2 (Fig. 1). Due to donor availability, the lowest instrumented segment was L3. Further specifications of the preparations of the cadaveric spine segments can be found in the study by Doodkorte et al. (Doodkorte et al., 2021b) Instrumentation constructs were chosen based on previous studies, from which these techniques were copied (Doodkorte et al., 2021a). All conditions were subjected to four cycles of ±5 Nm loading in flexion-extension and lateral bending. Segmental RoM was calculated in each test. Prior to biomechanical testing of the spine, the seven spines tested were graded for their level of IVD degeneration using the 8-level modified Pfirrmann grading scale (Griffith et al., 2007).

2.2. Parametric finite element model

A parametric FE model, originally developed by Meijer (Meijer, 2011) and later on validated by Roth et al. (Roth et al., 2021), was used to simulate the experiments (Fig. 2A). The geometry of the vertebrae varies along the spine based upon the position of the endplates (Langrana et al., 2006; Mizrahi et al., 1993). The facet joints have been implemented as two parallel surfaces with a distance of 0.6 mm in between. To account for the reduced stiffness of the ligaments towards the cranial levels a gradient was applied to the cross-sectional area (CSA) of most ligaments (Table 1) (Roth et al., 2021). Material properties of the other structures are shown in Table 2. Isotropic linear elastic material properties were defined for the vertebral body, posterior elements and endplates. To account for their typical nonlinear behavior, the nucleus pulposus and annulus fibrosus ground substance were modelled as hyperelastic solids, as described by incompressible Mooney-Rivlin equations. Annulus fibers are included by linear elastic, tension-only rebar elements. These fibers are oriented at +30° and −30° respective to the transverse plane, with a 16% volume ratio. The non-linear behavior of the ligaments is defined by a piecewise linear-elastic equation, with different stiffness properties in three regions (Table 1). For the facet joints, frictional contact was defined with friction coefficient 0.01.

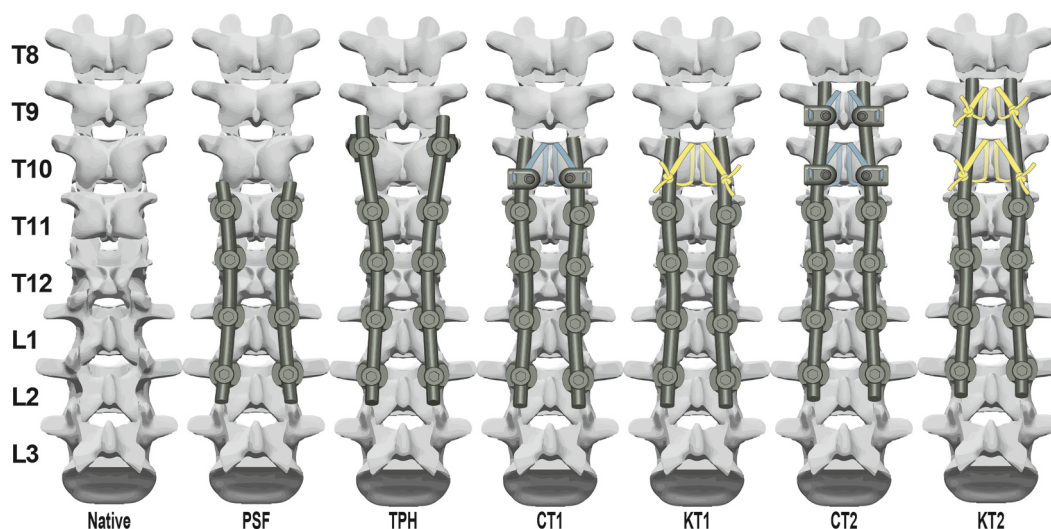**Fig. 1.** In the *ex vivo* experiment, the human cadaveric spine segments were instrumented with; three-level pedicle screw fixation (PSF) and subsequently tested with transverse hooks (TPH), one- and two-level clamped sublaminar tape (CT1 and CT2), and knotted sublaminar tape (KT1 and KT2) as semi-rigid junctional fixation. Reprinted from Doodkorte et al. (2021a), with permission from Elsevier.
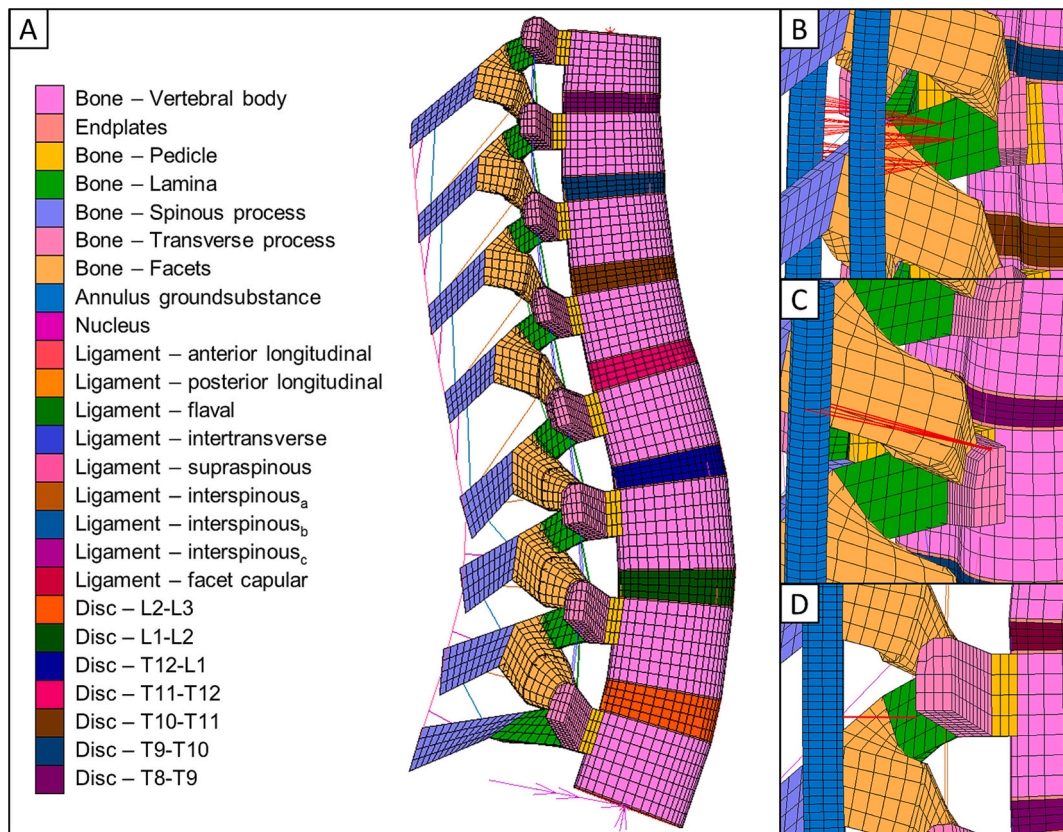
Fig. 2. A) Spinal FE model of segmental levels T8-L3, based on a healthy mature spine; B) Pedicle screw fixation modelled as three rigid body connection connecting the lamina and rod at the UIV; C) Transverse process hook modelled as one rigid body connection connecting the transverse process to the rod at the UIV + 1; D) Tape modelled as a single line element for each tape connecting the lamina to the rod at the UIV + 1).

Table 1
Material properties of the ligament. ALL = anterior longitudinal ligament, PLL = posterior longitudinal ligament, CL = facet joint capsular ligaments, ITL = intertransverse ligaments, FL = flaval ligament, ISL = interspinous ligament, SSL = supraspinous ligament (SSL), CSA = cross sectional area.

Ligament	CSA [mm^2]			Region 1		Region 2		Region 3	
	L2-L3	step/ level	T8-T9	Strain [−]	E [MPa]	Strain [−]	E [MPa]	Strain [−]	E [MPa]
ALL	61	5	31	0.00–0.12	24.1	0.12–0.45	90.7	0.45–0.58	45.2
PLL	25	1	19	0.00–0.09	19.2	0.09–0.34	181.5	0.34–0.45	58.5
CL	38	1	32	0.00–1.00	0.96	1.00–2.00	19.2	2.00–3.00	6.4
ITL	39	1	33	0.00–0.09	34.2	0.09–0.15	335.7	0.15–0.17	112.7
FL	29	1	23	0.00–0.05	5.0	0.05–0.50	13.1	0.50–0.58	4.0
ISL	2	–	2	0.00–0.12	1.2	0.12–0.30	5.3	0.30–0.40	2.5
SSL	30	–	30	0.00–0.12	1.8	0.12–0.30	8.0	0.30–0.40	3.8

Ligament material properties derived from: (Chazal et al., 1985), (Goel et al., 1995), (Heuer et al., 2007), (Meijer, 2011), (Roth et al., 2021)

2.3. Modelling disc degeneration

In order to represent the spine segments used in the previous experiments as accurately as possible, disc degeneration of the seven experimentally used spine segments was implemented *in silico* by reducing IVD height. The modified MRI-based Pfirrmann grades of the individual IVDs were interpolated to a 4-level scale (0–3) to allow for translation to the radiographic classification system proposed by Kettler et al. (Kettler et al., 2011) This classification system incorporates disc height reduction and therefore allows for back-translation of IVD scoring to disc height reduction. We assumed that grade 1, 2, and 3 correspond to a reduction of IVD height by 16.5%, 49.5%, and 82.5% of the original height similar to Schmidt et al. (Schmidt et al., 2007) In the subsequent validation of the semi-rigid junctional fixation techniques, the IVD grade of the seven cadavers (T8-L3) was averaged for each IVD level and adapted into the FE model as described above, creating a single

average 'degenerative' FE model.

2.4. Implementing semi-rigid junctional fixation techniques

Bilateral spinal rods were introduced as modelled by Meijer (Meijer, 2011). Material properties for the spinal rods were assigned to correspond with the titanium rods used in the biomechanical experiment by Doodkorte et al. (Doodkorte et al., 2021b) (Ø5.50 mm, E = 110 GPa, $\nu =$ 0.3).

PSF was modelled as a rigid body connection between the lamina and the rod (Fig. 2B). A single pedicle screw was modelled as three rigid body connections to constrain rotation of the rod in all directions. The TPH was modelled as a rigid body connection between the most lateral point of the transverse process to four coplanar points located on the rod, thereby allowing rotational degrees of freedom at the side of the bone (Fig. 2C). Each tape (CT1, KT1, CT2 and KT2) was modelled as a

Table 2

Material properties of the parametric spinal FE model.

Anatomical structure	Material properties type	Values	References
Vertebral body	Isotropic linear elastic	E = 3 GPa, ν = 0.3	(Shirazi-Adl and Drouin, 1988) (Schmidt et al., 2007)
Vertebral posterior elements	Isotropic linear elastic	E = 3 GPa, ν = 0.3	(Goel et al., 1995) (Schmidt et al., 2006)
Endplates	Isotropic linear elastic	E = 50 MPa, ν = 0.25	(Lu et al., 1996)
Annulus fibers	Linear elastic, Tension-only rebar elements	E = 1.2 GPa, ν = 0.3	(Roth et al., 2021) (Heuer et al., 2007) (Schmidt et al., 2006)
Annulus groundsubstance	Mooney-Rivlin	C10 = 0.08 MPa, C01 = 0.02 MPa	(Mizrahi et al., 1993) (Benneker et al., 2005) (Fujiwara et al., 1999)
Nucleus pulposus	Mooney-Rivlin	C10 = 0.12 MPa, C01 = 0.09 MPa	(Schmidt et al., 2006)

single elastic isotropic actuator element connecting the lamina to the rod at the superior end of the lamina, with rotational degrees of freedom at both ends (Fig. 2D). Based on literature data describing the mechanical behavior of the fully secured sublaminar cable systems (Mazda et al., 2009; Roth et al., 2018), Young's Moduli were set at 21.9 GPa for KT and 36.1 GPa for CT, respectively. The CSA was set to 1.28 mm^2 for KT (representing a double loop) and 0.64mm^2 for CT (representing a single loop). In case of sublaminar tape fixation, surgical resection of flaval ligaments was represented by removal of the corresponding elements.

In the *ex vivo* experiment, a pre-tension of 700 N and 500 N was applied on the sublaminar tape for CT and KT, which after initial tension loss, a common phenomenon (Menard Jr. et al., 2013), results in approximately 300-500 N and 50-100 N internal loop tension, respectively (internal laboratory observation). In the FE model, the sublaminar tapes were represented by actuator elements and pre-tensioning was simulated by reducing the element length prior to simulating pure moment loading. The required actuator element shortening was determined iteratively until the desired pre-tension was reached. An average pre-tension of 380 N and 90 N was applied for the CT and KT, respectively.

2.5. Simulations

All simulations were performed in Marc Mentat (version 2014.0.0, MSC Software Corporation, Newport Beach, CA). Each model was tested in flexion-extension and lateral bending by applying a moment of 5 Nm in each direction. The caudal endplate of the spine segment was constrained for all displacements and rotations. The moment was applied to the cranial endplate of the T8 vertebra in 50 increments, while displacement constraining boundary conditions were applied to ensure bending in one plane only (*i.e.* a restriction in lateral direction in case of flexion-extension and a restricting in anterior-posterior movement in case of lateral bending).

2.6. Analysis

The segmental RoM of the seven FE models with patient-specific IVD degeneration, but without instrumentation, were compared to the results of the native condition of the biomechanical experiment with a paired-samples *t*-test using SPSS statistics software (SPSS 25; IBM, Chicago, IL). Bonferroni correction was applied to account for multiple comparisons. Furthermore, the results of the seven degenerative FE models were compared to the results of the original 'healthy' model and the average 'degenerative' FE model.

Segmental RoMs of the instrumented conditions were normalized to the non-instrumented RoMs identical to the biomechanical experiment (Doodkorte et al., 2021b). The highly stable construct along the thoracolumbar junction allowed for isolated evaluation of the cranial segments of the semi-rigid junctional fixation. Therefore, for comparison of the FE model to the *ex vivo* experiment, special interest was given to the semi-rigid fixation levels T10-T11 (index motion segment) and T9-T10 (the index+1 motion segment). Forces in the PLC (average ISL and SSL) and average Von Mises Stress (VMS) in the IVD (mean of nucleus pulposus elements) were measured at ultimate flexion and normalized to the non-instrumented FE model. The transition of PLC forces and nucleus pulposus (NP) VMS across the junctional zone were qualitatively analyzed.

3. Results

3.1. Disc degeneration

Implementing IVD height decrease as a means to represent the degenerative spine had a substantial effect on segmental RoM in both flexion-extension and lateral bending, which is especially noticeable in the thoracic spine (Fig. 3A,B). The mean of the seven individual degenerative FE models approximated the *ex vivo* results very well, as no significant difference was found between the mean RoM of the seven degenerative FE models and the *ex vivo* RoM for the native spine condition at any level ($p > 0.05$). Finally, the average degenerative FE model provided a valid representation for the mean of the seven degenerative models as only minute differences ($<5\%$) were obtained between the mean RoM values of the seven degenerative models and the average degenerative model. For this reason, the average degenerative model was used for all subsequent simulations.

3.2. Semi-rigid junctional fixation implementation

Excellent agreement between the *ex vivo* normalized RoM (nRoM) and *in silico* nRoM was attained for the instrumented conditions along the complete spine segment (Fig. 4). At the junctional zone, we observed that the *in silico* nRoM mostly falls within the first and third quartile of the experimental data in flexion-extension. The nRoMs for CT1 at the index+1 motion segment and CT2 at the index motion segment are outside the 95% CI, but still in the same ranking in relation to the other modelled conditions. Still focusing on the junctional zone, but in lateral bending, the *in silico* nRoMs lie within the first and third quartile of the *ex vivo* nRoMs, except for underestimations of TPH, CT1, CT2 and KT1 at level T11-T12 (of which only TPH is outside the 95% CI).

Outside the junctional zone, almost all *in silico* nRoMs lie within the 25th–75th percentile of the *ex vivo* nRoMs. Notable exceptions in flexion-extension are an underestimation of the nRoM by the FE model at T8-T9 for the KT and CT conditions. In lateral bending, the nRoM is slightly overestimated at level L1-L2 for all conditions except KT2 (outside the 95% CI for PSF) and above the mean for all conditions.

Compared to the native spine, PSF reduced the PLC forces by 98% at index-1, but an increase to 108% was observed at the index segment (Fig. 5A). All semi-rigid junctional fixation techniques reduced the PLC forces at the junctional zone compared to PSF. TPH showed the most gradual change in PLC forces, over two motion segments, with the forces reduced to 52% at the index as compared to the native spine. KT1 resulted in a slightly less gradual change, with PLC forces of 12% at the index. KT2 completely unloaded the PLC at the index and rendered forces of 65% at the index+1. Both CT1 and CT2 took over 100% of the PLC forces at the index and around 50% at the index+1, thus creating the same gradual change as TPH, but requiring an extra motion segment for a gradual transition of PLC forces.

Regarding the IVD, the TPH and KT1 reduced the stresses in the NP almost by half at the index level to 48% and 55%, respectively (Fig. 5B). KT2 reduced the NP VMS to 41% at index and 51% and index+1.
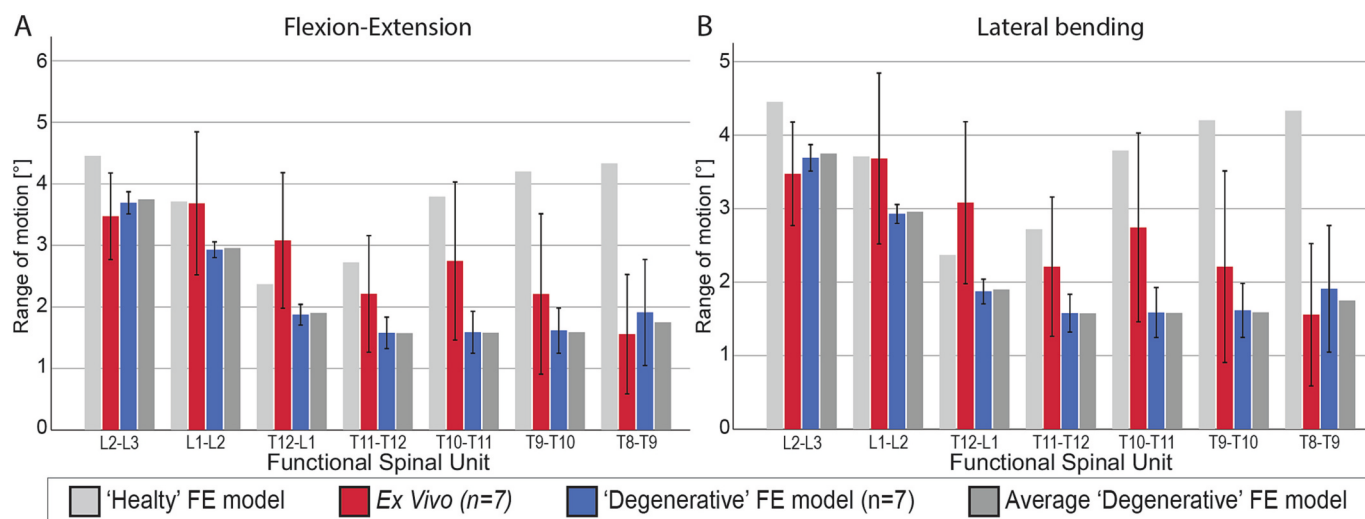
Fig. 3. Segmental range of motion in flexion-extension (A) and lateral bending (B) of the 'healthy' FE model, the *ex vivo* measurements, the seven 'degenerative' models (mean ± 1SD) and the average 'degenerative' model.

Strikingly, the stress in the NP for both CT1 and CT2 increased to 199% and 195% at the T11-T12 and 124% and 134% at the index level, respectively. This elevated NP stress was also present at index+1 for CT2 (104%).

4. Discussion

PJK and PJF are major complications following surgical treatment of ASD correction using long segmental PSF (Kim et al., 2012). A gradual change in RoM in the junctional zone should lead to a gradual change in stresses, and thereby a reduced risk for PJK (Ou-Yang et al., 2020). In the current study, we successfully implemented IVD degeneration into an existing parametric spinal FE model to replicate *ex vivo* results obtained with human cadaveric material (Meijer, 2011; Roth et al., 2021). Subsequently, five different semi-rigid junctional fixation techniques were validated against experimental data from an *ex vivo* human cadaveric experiment by Doodkorte et al. (Doodkorte et al., 2021b) only for pure flexion-extension and lateral bending movement. Finally, the transitions in PLC forces and NP VMS did not scale proportionally with the nRoM transition for various semi-rigid junctional fixation techniques.

Considering PJK is a forward decompensation of the spine, the nRoM and stresses in the PLC and NP in flexion were of primary interest (Bess et al., 2017). In case of PSF, forces in the PLC showed a similar abrupt increase as observed for the nRoM at the proximal end of the PSF. All semi-rigid junctional fixation techniques reduced PLC forces at the junctional zone as compared to PSF. TPH showed the most gradual change in PLC forces at the junctional zone over two spinal levels, as was also observed for nRoM, followed by KT1. Strikingly, CT1 and CT2 showed the same change in forces as TPH. However, the transition zone was shifted one level up, a pattern similar to the shifted nRoM transition zone of CT2. PCL forces were mitigated by KT2 on the index level, which is not reflected by the nRoM. Clearly, the nRoM reduction is not proportional to the percentage force reduction in the PLC. Previous studies showed that the large forces used to tension tethers also resulted in complete unloading of the PLC (Buell et al., 2019). Complete unloading of the PLC at the index and ~50% unloading at the index+1 corresponds to the relatively rigid kinematic behavior of CT fixation.

When evaluating the NP stresses, it appears that KT1, KT2 and TPH reduce the stresses in the IVD substantially, but to a different extent. The transition in NP stresses are also not directly proportional to the nRoM transition, as was previously noted by Buell et al. (Buell et al., 2019) Strikingly, CT1 and CT2 conditions increased instead of decreased NP stresses at the junctional zone. Cho et al. (Cho et al., 2018) measured an

increased lordosis angle with posterior tension band instrumentation, with higher forces resulting in increasing angles in a human cadaveric experiment. Similarly, the high tension forces used in CT instrumentation resulted in the posterior translation of the index (and index+1) vertebrae in the current model. Therefore, CT techniques appear to disrupt the interplay between the anterior and posterior column of the spine. The exact contribution of each tissue of the spinal motion segment in the development of PJF is yet to be established. Following this implementation validation study, application of a hybrid testing protocol to the developed FE models, as described by Panjabi (Panjabi, 2007), allows for further investigation of the individual tissue contributions. Furthermore, the clinical implications of the non-proportional relation between nRoM and stresses over the junctional zone are still to be determined. A prospective analysis of patients treated with the different studied techniques comparing the effectiveness on preventing PJK would be the next step in research. Data from such a trial is crucial to elucidate the importance of these numerical findings and to compare the effectiveness of the semi-rigid junctional fixation techniques in terms of reducing PJK/PJF incidence rates.

The FE model clearly showed the stable thoracolumbar junction and abrupt increase in nRoM at the proximal end of the PSF. The nRoM results of FE models including the semi-rigid junctional fixation instrumentation in flexion-extension and lateral bending were in good agreement with the *ex vivo* data. Specifically, most *in silico* nRoM results lay within the 25th and 75th percentile of the biomechanical experiment with some specific exceptions, notably for the CT conditions. In case of flexion, the model underestimated nRoMs for CT1 at index+1 and T8-T9 and KT and CT at T8-T9. It must be noted that the nRoMs for the experimental data were above 1.0. This discrepancy was previously discussed by Doodkorte et al. (Doodkorte et al., 2021b) and is more likely to be an experimental artefact rather than a model error. In lateral bending, the FE model slightly underestimates the nRoM for most instrumentations at the index motion segment. This may be due to constrained out-of-plane movements in the FE model together with the asymmetry of the cadaveric spines *i.e.*, the spine was experimentally allowed out of plane movements during the lateral bending test, which were constrained *in silico*. Despite the abovementioned differences between the FE model and the *ex vivo* experiment, the majority of the results was in agreement and no difference in ranking between the semi-rigid junctional fixation with respect to nRoM was measured. Therefore, the results presented herein may be considered representative.

IVD degeneration was implemented in the FE model by reducing the height of the IVD based on the modified Pfirrmann grading scale of the
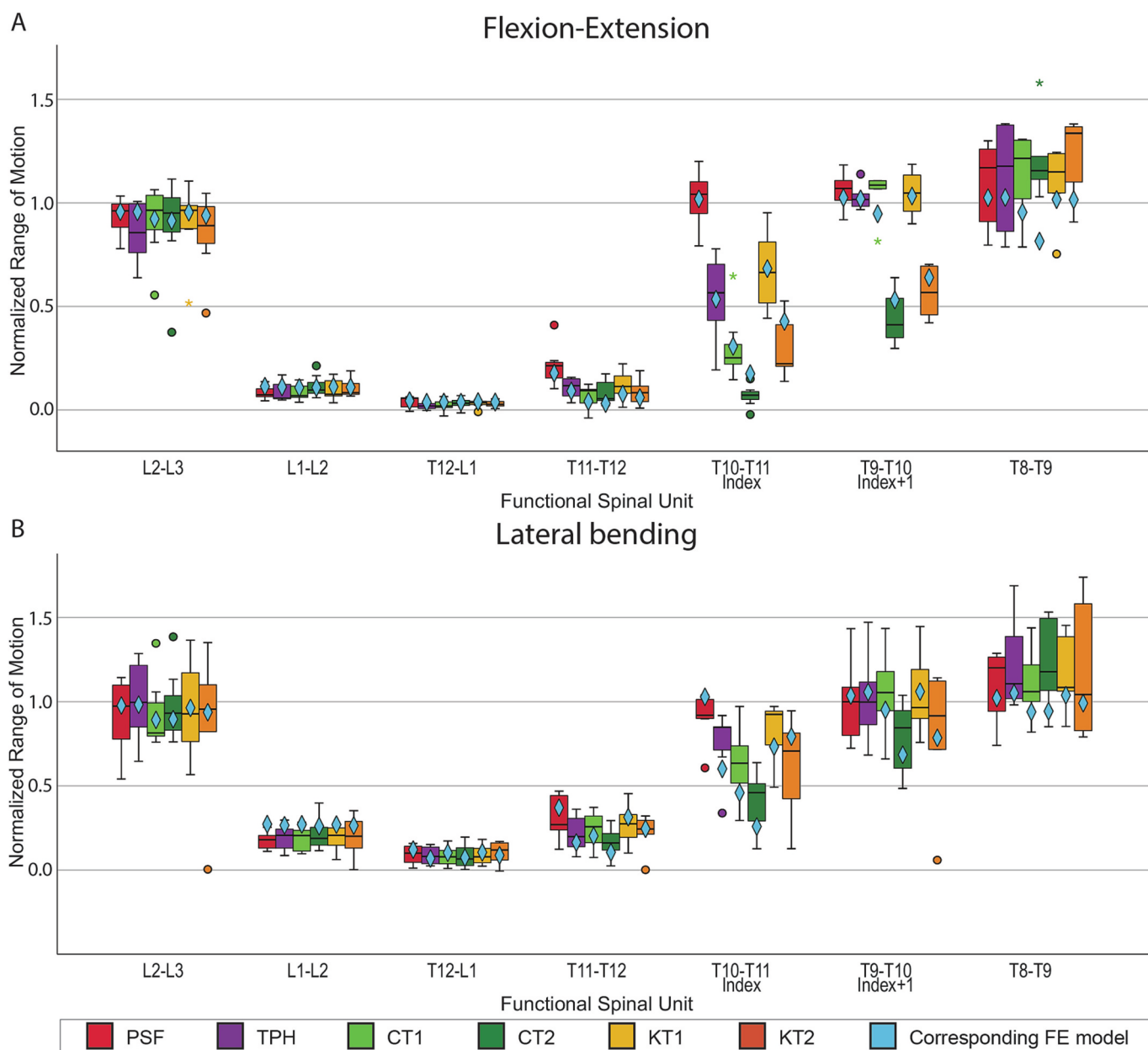
Fig. 4. Normalized range of motion in flexion-extension (A), and lateral bending (B). Boxplots include the mean and interquartile range from T11-T12, the most proximal PSF instrumented level, to T9-T10, the index+1. Blue rhombuses indicate the results of the FE simulations for each corresponding instrumentation. Native) uninstrumented spine, PSF) three level pedicle screw fixation, TPH) transverse process hook, CT1) 1 level sublaminar clamped tape, CT2) 2 level sublaminar clamped tape, KT1) 1 level knotted sublaminar tape, KT2) 2 level knotted sublaminar tape. (For interpretation of the references to colour in this figure legend, the reader is referred to the web version of this article.)

cadaveric spine segments in accordance with Kettler et al. (Kettler et al., 2011) and no material properties were adapted for the degenerative FE model. The latter was because the Pfirrmann grade can only provide very limited information about the material properties of the disc, while disc height is better quantifiable and has a major influence on the RoM (Meijer, 2011). It should be noted that the stresses in the disc are less affected by this limitation as these are determined mainly by the applied force/moment and cross-sectional geometry.

Strikingly, the *ex vivo* data showed an elevated RoM at level T10-T11 as compared to the surrounding segments. Other experimental data shows a more gradual decrease in RoM from L3 towards T8, just like the seven 'degenerative' FE models (White and Panjabi, 1978; Wilke et al., 2017). Although the (non-significant) discrepancy at the T12-L1 level between the 'degenerative' FE model and the *ex vivo* results must be

pointed out, this was of no concern for the instrumentation comparison considering that level is the most stable fusion level in all conditions. The average 'degenerative' FE model shows excellent agreement with the mean of the seven FE models of the cadavers. This average 'degenerative' model was therefore considered valid for the implementation of the semi-rigid junctional fixation.

The simplifications made whilst implementing the instrumentation should be considered. The tapes were modelled as actuators in order to apply pre-tension, preventing the tapes from being compressible. This might have affected RoM calculations, especially in extension and in application of the pretension for two-level sublaminar tape fixation. Further development of the model could explore implementing the tape as an actuator in series with a non-linear tension-only element. Furthermore, the current instrumentation techniques might be
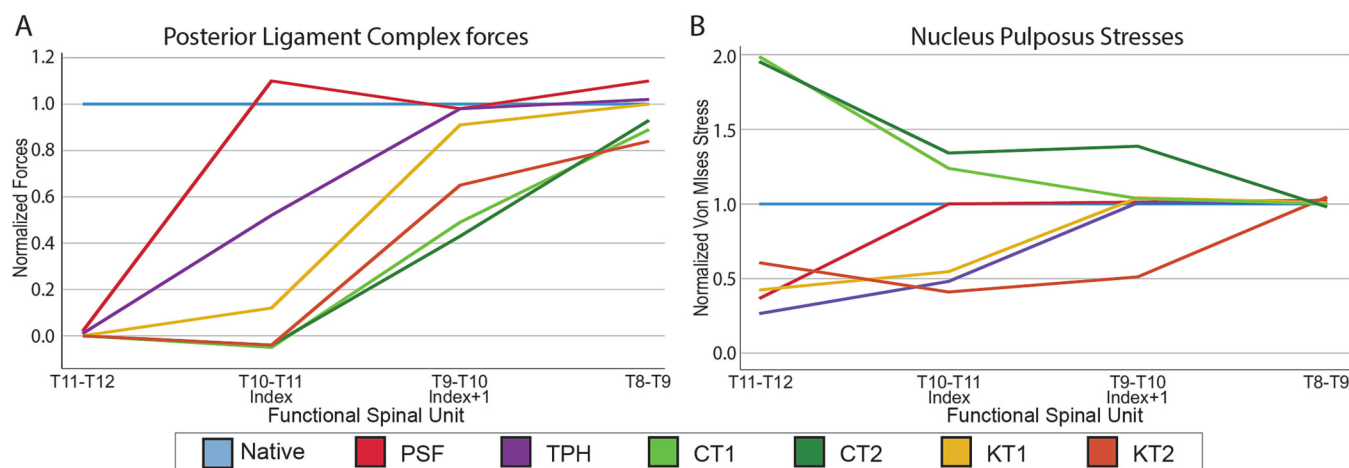
Fig. 5. Normalized average VMS in the posterior ligament complex (A) and nucleus pulposus (B) for the different techniques over the junctional zone.

compared to less invasive techniques, like the recent Novel Cable Anchor System (Doodkorte et al., 2022). Finally, the NP and annulus fibrosus were modelled as hyperplastic solids rather than as poro-elastic, preventing calculation of true hydrostatic intradiscal pressures. Hence, the current study presented the VMS in the NP, limiting comparison to relevant *ex vivo* intradiscal pressure measurements and translation towards PJK/PJF risk. Despite these simplifications, the nRoMs of the FE model were highly comparable to the biomechanical results and a non-linear relation between nRoM transition zones and the transition of stresses over the same zone was demonstrated.

5. Conclusion

The RoMs calculated from the FE model were in close agreement with the biomechanical results for all semi-rigid junctional fixation instrumentation types, in both lateral bending and in flexion-extension. The transition in the PLC and NP stresses were not always proportional to the nRoM transition, *i.e.* a smooth nRoM transition zone does not directly imply a smooth transition in stresses. Prospective evaluation, subjecting each of the semi-rigid junctional fixation techniques to the same rotation, and a robust clinical trial are required for the translation of the findings into clinical applicability.

Author contribution

JvA made substantial contributions to the concept, design, and execution of the modelling process, to the acquisition, analysis and interpretation of data, and to drafting the paper.

RD made substantial contributions to the concept of the models, execution of the biomechanical experiment, to the analysis and interpretation of data, and to revision of the paper. BvR made substantial contributions to the concept, design, and solving of technical challenges during the modelling process, and the revision of the manuscript. AR, KI, PW, and JA made substantial contributions to the revision of the manuscript.

All authors have read and approved the final manuscript.

Declaration of Competing Interest

The authors declare that they have no known competing financial interests or personal relationships that could have appeared to influence the work reported in this paper.

Acknowledgments

This research was performed under the framework of Chemelot

References

Benneker, L.M., Heini, P.F., Anderson, S.E., et al., Feb 2005. Correlation of radiographic and MRI parameters to morphological and biochemical assessment of intervertebral disc degeneration. Eur. Spine J. 14 (1), 27–35. https://doi.org/10.1007/s00586-004-0759-4.

Bess, S., Harris, J.E., Turner, A.W., et al., Jan 2017. The effect of posterior polyester tethers on the biomechanics of proximal junctional kyphosis: a finite element analysis. J Neurosurg Spine. 26 (1), 125–133. https://doi.org/10.3171/2016.6.SPINE151477.

Buell, T.J., Bess, S., Xu, M., et al., Feb 8, 2019. Optimal tether configurations and preload tensioning to prevent proximal junctional kyphosis: a finite element analysis. J Neurosurg Spine. 1–11. https://doi.org/10.3171/2018.10.SPINE18429.

Cahill, P.J., Wang, W., Asghar, J., et al., May 20, 2012. The use of a transition rod may prevent proximal junctional kyphosis in the thoracic spine after scoliosis surgery: a finite element analysis. Spine (Phila Pa 1976) 37 (12), E687–E695. https://doi.org/10.1097/BRS.0b013e318246d4f2.

Chazal, J., Tanguy, A., Bourges, M., et al., 1985. Biomechanical properties of spinal ligaments and a histological study of the supraspinal ligament in traction. J. Biomech. 18 (3), 167–176. https://doi.org/10.1016/0021-9290(85)90202-7.

Cho, S.K., Caridi, J., Kim, J.S., et al., Dec 2018. Attenuation of proximal junctional kyphosis using sublaminar polyester tension bands: a biomechanical study. World Neurosurg. 120, e1136–e1142. https://doi.org/10.1016/j.wneu.2018.08.244.

DeWald, C.J., Stanley, T., Sep 1, 2006. Instrumentation-related complications of multilevel fusions for adult spinal deformity patients over age 65: surgical considerations and treatment options in patients with poor bone quality. Spine (Phila Pa 1976) 31 (19 Suppl), S144–S151. https://doi.org/10.1097/01.brs.0000236893.65878.39.

Doodkorte, R.J.P., Vercoulen, T.F.G., Roth, A.K., et al., 2021a. Instrumentation techniques to prevent proximal junctional kyphosis and proximal junctional failure in adult spinal deformity correction-a systematic review of biomechanical studies. Spine J. 21 (5), 842–854. https://doi.org/10.1016/j.spinee.2021.01.011.

Doodkorte, R.J.P., Roth, A.K., Arts, J.J., et al., 2021b. Biomechanical comparison of semi-rigid junctional fixation techniques to prevent proximal junctional failure after thoracolumbar adult spinal deformity correction. Spine J. 21 (5), 855–864. https://doi.org/10.1016/j.spinee.2021.01.017.

Doodkorte, R.J., Roth, A.K., Jacobs, E., et al., May 01, 2022. Biomechanical evaluation of semi-rigid junctional fixation using a novel cable anchor system to prevent proximal junctional failure in adult spinal deformity surgery. Spine. 47 (9), E415–E422. https://doi.org/10.1097/BRS.0000000000004228.

Fujiwara, A., Tamai, K., Yamato, M., et al., 1999. The relationship between facet joint osteoarthritis and disc degeneration of the lumbar spine: an MRI study. Eur. Spine J. 8 (5), 396–401. https://doi.org/10.1007/s005860050193.

Glattes, R.C., Bridwell, K.H., Lenke, L.G., et al., Jul 15, 2005. Proximal junctional kyphosis in adult spinal deformity following long instrumented posterior spinal fusion: incidence, outcomes, and risk factor analysis. Spine (Phila Pa 1976) 30 (14), 1643–1649. https://doi.org/10.1097/01.brs.0000169451.76359.49.

Goel, V.K., Monroe, B.T., Gilbertson, L.G., Brinckmann, P., Mar 15, 1995. Interlaminar shear stresses and laminae separation in a disc. Finite element analysis of the L3-L4 motion segment subjected to axial compressive loads. Spine (Phila Pa 1976) 20 (6), 689–698.

Griffith, J.F., Wang, Y.X., Antonio, G.E., et al., Nov 15, 2007. Modified Pfirrmann grading system for lumbar intervertebral disc degeneration. Spine (Phila Pa 1976). 32 (24) https://doi.org/10.1097/BRS.0b013e31815a59a0. E708–12.

Heuer, F., Schmidt, H., Klezl, Z., et al., 2007. Stepwise reduction of functional spinal structures increase range of motion and change lordosis angle. J. Biomech. 40 (2), 271–280. https://doi.org/10.1016/j.jbiomech.2006.01.007.

Kettler, A., Rohlmann, F., Ring, C., et al., Apr 2011. Do early stages of lumbar intervertebral disc degeneration really cause instability? Evaluation of an in vitro database. Eur. Spine J. 20 (4), 578–584. https://doi.org/10.1007/s00586-010-1635-z.

Kim, Y.J., Bridwell, K.H., Lenke, L.G., et al., Sep 15, 2005. Proximal junctional kyphosis in adolescent idiopathic scoliosis following segmental posterior spinal instrumentation and fusion: minimum 5-year follow-up. Spine (Phila Pa 1976) 30 (18), 2045–2050. https://doi.org/10.1097/01.brs.0000179084.45839.ad.

Kim, H.J., Lenke, L.G., Shaffrey, C.I., et al., Oct 15, 2012. Proximal junctional kyphosis as a distinct form of adjacent segment pathology after spinal deformity surgery: a systematic review. Spine (Phila Pa 1976) 37 (22 Suppl) https://doi.org/10.1097/BRS.0b013e31826d611b. S144–64.

Langrana, N.A., Kale, S.P., Edwards, W.T., et al., May–Jun 2006. Measurement and analyses of the effects of adjacent end plate curvatures on vertebral stresses. Spine J. 6 (3), 267–278. https://doi.org/10.1016/j.spinee.2005.09.008.

Lu, Y.M., Hutton, W.C., Gharpuray, V.M., Oct 1, 1996. Can variations in intervertebral disc height affect the mechanical function of the disc? Spine (Phila Pa 1976). 21 (19), 2208–2216 discussion 2217. https://doi.org/10.1097/00007632-199610010-00006.

Mazda, K., Ilharreborde, B., Even, J., et al., Feb 2009. Efficacy and safety of posteromedial translation for correction of thoracic curves in adolescent idiopathic scoliosis using a new connection to the spine: the universal clamp. Eur. Spine J. 18 (2), 158–169. https://doi.org/10.1007/s00586-008-0839-y.

Meijer, G.J.M., 2011. Development of a non-fusion scoliosis correction device. In: Numerical Modelling of Scoliosis Correction.

Menard Jr., J., Emard, M., Canet, F., et al., Oct 2013. Initial tension loss in cerclage cables. J. Arthroplast. 28 (9), 1509–1512. https://doi.org/10.1016/j.arth.2013.03.014.

Mizrahi, J., Silva, M.J., Keaveny, T.M., et al., Oct 15 1993. Finite-element stress analysis of the normal and osteoporotic lumbar vertebral body. Spine (Phila Pa 1976). 18 (14), 2088–2096. https://doi.org/10.1097/00007632-199310001-00028.

Ou-Yang, D., Moldavsky, M., Wessell, N., et al., Aug 2020. Evaluation of spinous process tethering at the proximal end of rigid constructs: in vitro range of motion and intradiscal pressure at instrumented and adjacent levels. Int J Spine Surg. 14 (4), 571–579. https://doi.org/10.14444/7076.

Panjabi, M.M., Mar 2007. Hybrid multidirectional test method to evaluate spinal adjacent-level effects. Clin. Biomech. 22 (3), 257–265. https://doi.org/10.1016/j.clinbiomech.2006.08.006.

Roth, A.K., Boon-Ceelen, K., Smelt, H., et al., Feb 2018. Radiopaque UHMWPE sublaminar cables for spinal deformity correction: preclinical mechanical and radiopacifier leaching assessment. J Biomed Mater Res B Appl Biomater 106 (2), 771–779. https://doi.org/10.1002/jbm.b.33886.

Roth, A.K., Beheshtiha, A.S., van der Meer, R., et al., May 2021. Validation of a finite element model of the thoracolumbar spine to study instrumentation level variations in early onset scoliosis correction. J. Mech. Behav. Biomed. Mater. 117, 104360 https://doi.org/10.1016/j.jmbbm.2021.104360.

Schmidt, H., Heuer, F., Simon, U., et al., May 2006. Application of a new calibration method for a three-dimensional finite element model of a human lumbar annulus fibrosus. Clin. Biomech. 21 (4), 337–344. https://doi.org/10.1016/j.clinbiomech.2005.12.001.

Schmidt, H., Kettler, A., Rohlmann, A., et al., Nov 2007. The risk of disc prolapses with complex loading in different degrees of disc degeneration - a finite element analysis. Clin. Biomech. 22 (9), 988–998. https://doi.org/10.1016/j.clinbiomech.2007.07.008.

Shirazi-Adl, A., Drouin, G., Aug 1988. Nonlinear gross response analysis of a lumbar motion segment in combined sagittal loadings. J. Biomech. Eng. 110 (3), 216–222. https://doi.org/10.1115/1.3108434.

Silva, F.E., Lenke, L.G., Mar 2010. Adult degenerative scoliosis: evaluation and management. Neurosurg. Focus. 28 (3), E1. https://doi.org/10.3171/2010.1.FOCUS09271.

Spina, N.T., Abiola, R., Lawrence, B.D., 2017. Proximal junctional failure in adult spinal deformity surgery: incidence, risk factors, and management. Oper. Tech. Orthop. 27 (4), 251–259. https://doi.org/10.1053/j.oto.2017.09.009.

White, A.A., Panjabi, M.M., 1978. Clinical Biomechanics of the Spine. Lippincott.

Wilke, H.J., Herkommer, A., Werner, K., Liebsch, C., 2017. In vitro analysis of the segmental flexibility of the thoracic spine. PLoS One 12 (5), e0177823. https://doi.org/10.1371/journal.pone.0177823.

Yagi, M., Akilah, K.B., Boachie-Adjei, O., Jan 1, 2011. Incidence, risk factors and classification of proximal junctional kyphosis: surgical outcomes review of adult idiopathic scoliosis. Spine (Phila Pa 1976). 36 (1), E60–E68. https://doi.org/10.1097/BRS.0b013e3181eeaee2.